Mode-locking of monolithic laser diodes incorporating coupled-resonator optical waveguides

Yang Liu, Zheng Wang, Minghui Han, Shanhui Fan, and Robert Dutton

Integrated Circuits Laboratory and Gintzton Laboratory, Stanford University, Stanford, CA 94305

yangliu@gloworm.stanford.edu

Abstract: We investigate the operational principle of mode-locking in monolithic semiconductor lasers incorporating coupled-resonator optical waveguides. The size of mode-locked lasers operating at tens of GHz repetition frequencies can be drastically reduced owing to the significantly decreased group velocity of light. The dynamics of such devices are analyzed numerically based on a coupled-oscillator model with the gain, loss, spontaneous emission, nearest-neighbor coupling and amplitude phase coupling (as described by the linewidth enhancement factor α) taken into account. It is demonstrated that active mode-locking can be achieved for moderate α parameter values. Simulations also indicate that large α parameters may destabilize the mode-locking behavior and result in irregular pulsations, which nevertheless can be effectively suppressed by incorporating detuning of individual cavity resonant frequencies in the device design.

OCIS codes: (050.0050) Diffraction and gratings; (140.4050) Mode-locked lasers.

References and links

1. G. A. Keeler, B. E. Nelson, D. Agarwal, and D. A. B. Miller, "Skew and jitter removal using short optical pulses for optical interconnection," IEEE Photonics Technology Letters **12**, 714–716 (2000).
2. E. A. De Souza, M. C. Nuss, W. H. Knox, and D. A. B. Miller, "wavelength-division multiplexing with femtosecond pulses," Opt. Lett. **20**, 1166–1168 (1995).
3. E. A. Avrutin, J. H. Marsh, and E. L. Portnoi, "Monolithic and multi-GigaHertz mode-locked semiconductor lasers: constructions, experiments, models and applications," IEE Proc.-Optoelectron. **147**, 251–278 (2000).
4. A. E. Siegman, *Lasers* (University Science Books, Sausalito, CA, 1986).
5. N. Stefanou and A. Modinos, "Impurity bands in photonic insulators," Phys. Rev. B **57**, 12,127–12,133 (1998).
6. A. Yariv, Y. Xu, R. K. Lee, and A. Scherer, "Coupled-resonator optical waveguides: a proposal and analysis," Opt. Lett. **24**, 711–713 (1999).
7. M. Notomi, K. Yamada, A. Shinya, J. Takahashi, C. Takahashi, and I. Yokohama, "Extremely large group-velocity dispersion of line-defect waveguides in photonic crystal slabs," Phys. Rev. Lett. **87**, 253,902 (2001).
8. S. Olivier, C. Smith, M. Rattier, H. Benisty, C. Weisbuch, T. Krauss, R. Houdre, and U. Oesterle, "Miniband transmission in a photonic crystal coupled-resonator optical waveguide," Opt. Lett. **26**, 1019–1021, (2001).
9. S. Mookherjea and A. Yariv, "Optical pulse propagation in the tight-binding approximation," Opt. Express **9**, 91–96 (2001), http://www.opticsexpress.org/abstract.cfm?URI=OPEX-9-2-91.
10. M. Soljacic, S. G. Johnson, S. Fan, M. Ibanescu, E. Ippen, and J. D. Joannopoulos, "Photonic-crystal slow-light enhancement of nonlinear phase sensitivity," J. Opt. Soc. Am. B **19**, 2052–2059 (2002).
11. H. Altug and J. Vuckovic, "Two-dimensional coupled photonic crystal resonator arrays," Appl. Phys. Lett. **84**, 161–163 (2004).

#6747 - $15.00 USD Received 3 March 2005; revised 26 May 2005; accepted 31 May 2005

12. S. Mookherjea, "Semiconductor coupled-resonator optical waveguide laser," Appl. Phys. Lett. **84**, 3265–7 (2004).
13. D. Botez, "Monolithic phase-locked semiconductor laser arrays," in *Diode Laser Arrays*, D. Botez and D. R. Scifres, ed., pp. 1–67 (Cambridge University Press, New York, 1994).
14. S. S. Wang and H. G. Winful, "Dynamics of phase-locked semiconductor laser arrays," Appl. Phys. Lett. **52**, 1774–6 (1988).
15. H. G. Winful and S. S. Wang, "Stability of phase locking in coupled semiconductor laser arrays," Appl. Phys. Lett. **53**, 1894-6 (1988).
16. H. G. Winful and R. K. Defreez, "Dynamics of coherent semiconductor laser arrays," in *Diode Laser Arrays*, D. Botez and D. R. Scifres, ed., pp. 226–253 (Cambridge University Press, New York, 1994).
17. G. A. Wilson, R. K. DeFreez, and H. G. Winful, "Modulation of phased-array semiconductor lasers at K-band frequencies," IEEE J. Quantum Electron. **27**, 1696-1704, 1991.
18. H. G. Winful, S. Allen and L. Rahman, "Validity of the coupled-oscillator model for laser-array dynamics," Opt. Lett. **18**, 1810-2, 1993.
19. P. Ru, K. Jakobsen, J. V. Moloney, and R. A. Indik, "Generalized coupled-mode model for the multistripe index-guided laser arrays," J. Opt. Soc. Am. B **10**, 507-515, 1993
20. S. G. Johnson and J. D. Joannopoulos, "Block-iterative frequency-domain methods for Maxwell's equations in a planewave basis," Opt. Express **8**, 173–190 (2001), http://www.opticsexpress.org/abstract.cfm?URI=OPEX-8-3-173.
21. R. .J. Lang and A. Yariv, "Local-field rate equations for coupled optical resonators," Phys. Rev. A **34**, 2038-2043, 1986.
22. R. J. Lang and A. Yariv, "An exact formulation of coupled-mode theory for coupled-cavity lasers," IEEE J. Quantum Electron. **QE-24**, 66–72, 1988.
23. N. W. Ashcroft and N. D. Mermin, *Solid State Physics*, Ch. 10 (Saunders College Publishing, 1976).
24. C. H. Henry, "Line Broadening of Semiconductor Lasers," in *Coherence, Amplification, and Quantum Effects in Semiconductor Lasers*, Y. Yamamoto, ed., pp. 5–76 (Wiley, New York, 1991).
25. H. A. Haus, "Mode-locking of lasers," IEEE Journal of Selected Topics in Quantum Electronics **6**, 1173–1185 (2000).
26. L. A. Coldren and S. W. Corzine, *Diode Lasers and Photonic Integrated Circuits* (Wiley-Interscience, New York, 1995).
27. D. Marcuse, "Computer simulation of laser photon fluctuations: theory of single-cavity laser," IEEE J. Quantum Electron. **QE-20**, 1139–1148 (1984).
28. Y. Liu, K. D. Choquette, and K. Hess, "The electrical turn-on characteristics of vertical-cavity surface-emitting lasers," Appl. Phys. Lett. **83**, 4104–6 (2003).
29. J. Vuckovic, O. Painter, Y. Xu, A. Yariv, and A. Scherer, "Finite-difference time-domain calculation of the spontaneous emission coupling factor in optical microcavities," IEEE J. Quantum Electron. **35**, 1168–1175 (1999).
30. Y. Yu, G. Giuliani, and S. Donati, "Measurement of the linewidth enhancement factor of semiconductor lasers based on the optical feedback self-mixing effect," IEEE Photonic Technology Letters **16**, 990-992 (2004).

1. Introduction

The mode-locking behavior of lasers has long been a subject of extensive research efforts due to its key role in ultra-fast optics. Recently, it has triggered enormous research interest in optoelectronics for its potential applications in the optical clocking and optical interconnects in silicon-based integrated circuits. It was proposed that mode-locked laser pulses can be used to significantly suppress the jitter noise [1] and are compatible with the wavelength-division-multiplexing technique [2]. To exploit the benefit of those applications, the system integration considerations necessitate the use of monolithic laser diodes where mode-locking can be achieved in a compact, fully-integrated structure [3]. However, the physical length of the lasers imposes a fundamental constraint on the available repetition frequency range. In mode-locking operations, the repetition frequency f_r is simply related to the laser length L by $f_r = mv_g/(2L)$ [4] for a positive integer m ($m \geq 2$ is for higher-order harmonic mode-locking). Here, $v_g = c/n_r$ is the group velocity of light with the vacuum light speed $c = 3 \times 10^8 m/s$ and a typical III-V semiconductor refractive index $n_r \approx 3$. Therefore, for a repetition frequency around 10GHz that is compatible with typical optoelectronic components, the minimum physical length of mode-locked laser diodes is $5mm$. On the other hand, it is well established that by periodically modulating the optical dielectrics on a sub-wavelength scale, the group velocity of

#6747 - $15.00 USD Received 3 March 2005; revised 26 May 2005; accepted 31 May 2005

the light can be drastically reduced due to strong Bragg diffractions. This so-called "slow-light" property can be achieved in properly designed photonic crystals [5, 6, 7]. In this work, we propose the incorporation of such photonic structures into monolithic mode-locked laser diodes to drastically reduce the device size. For photonic crystals with openings of the photonic band-gap, extremely small group velocities typically occur at the band-edge states where the photon density of states is very high. However, very strong dispersion is also present in those regions, which limits the number of photon states available for mode-locking. Coupled-resonator optical waveguides (CROW) were proposed [5, 6] to achieve low group velocities in the defect bands, which has been experimentally verified [8]. The propagation of optical pulses in passive CROW structures has been analyzed in [9]. In CROW structures, the photon states in the middle of the defect bands have significantly reduced group velocity while still maintaining minimum dispersion. CROW structures have been proposed for Mach-Zehnder interferometers to reduce the device size significantly [10]. Two-dimensional CROW structures have also been designed and fabricated primarily for the reduction of laser threshold [11, 12].

There has been extensive work addressing phase-locked operation of coupled laser cavities [13]. The difference between phase-locking and mode-locking operations warrants a clarification here. For an array of optical resonators, the inter-cavity coupling in general leads to the formation of a frequency band composed of Eigen frequencies associated with the supermodes (also referred to as array modes or composite modes). The phase-locking operation generally refers to steady-state, single supermode lasing, preferably from either of the two band-edge supermodes (namely, the in-phase and out-of-phase supermodes) for good beam quality and high optical intensity. Stability analysis of phase-locking operations identified the competition between adjacent supermodes as a source of instability; irregular pulsations are generated as a result of their uncontrolled beating [14, 15, 16]. On the other hand, the mode-locking discussed in this work is to purposefully achieve simultaneous lasing and controlled beating (through modulated losses or saturable absorbers) of multiple supermodes in the middle of the band, which is manifested as an optical pulse periodically circulating in the array. In the work of Wilson et al. [17], the possibility of fast modulating coupled lasers at the beat frequency of their supermodes has been explored. However, they only analyzed the case of two cavities. The mode-locking behavior on the other hand, is only from the beating of multiple supermodes, which requires a sufficiently large number of cavities in the array. It exhibits qualitatively different dynamics compared to the two-cavity case.

In the following, we will demonstrate the principle of mode-locking in CROW laser structures using numerical analysis based on a coupled-oscillator model following the approach used in [16, 18, 19]. The model is based on the tight-binding approach and works best for index-guided, evanescently coupled arrays [18], as is the case in this work. The frequency-pulling effect due to amplitude phase coupling is modeled by the linewidth enhancement factor α. Based on this model, we simulate the transient dynamics of both photons and gain from turn-on to continuous-wave (cw) condition in the proposed devices. Simulation results demonstrate the occurrence of active mode-locking in such devices for moderate α parameters at repetition rates of $\sim 10GHz$, while the physical length of the device is reduced by more than an order of magnitude to ~ 100 micrometers. Further simulations with large α parameters reveal the negative impact of the amplitude phase coupling effect on the stability of mode-locking. Nevertheless, it is also found that even in that case, stable mode-locked operations can be recovered by incorporating detunings of individual cavity resonant frequencies in device design.

2. Theoretical models

Typical CROW structures [6, 11] can be readily tailored to suit the proposed mode-locked lasing operations; a schematic illustration of such structures is given in Fig. 1. The nominal lasing

#6747 - $15.00 USD Received 3 March 2005; revised 26 May 2005; accepted 31 May 2005

wavelength is $\lambda_0 = 850nm$. The active region of the laser is a single or multiple GaAs/AlGaAs

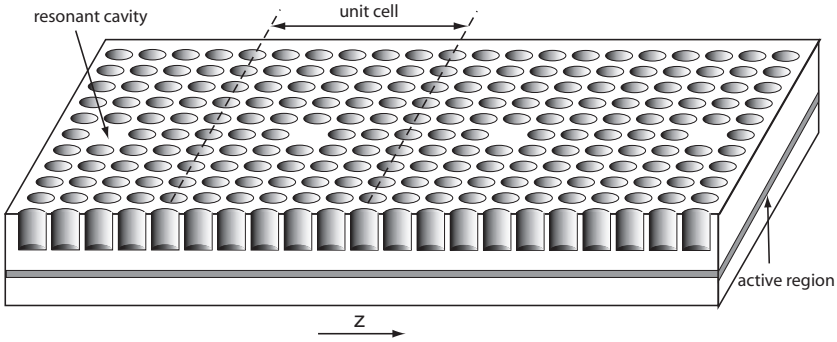

Fig. 1. Schematic plot of a typical CROW structure that is tailored for mode-locked lasing operations. The air holes in general need not to penetrate into the active region. The propagation direction is along the z-axis.

quantum well (QW) structure. To open a photonic band gap, a square lattice of air holes is etched into the top cladding layer to create the band-gap. A one-dimensional periodic array of defects are patterned along the lattice to form resonant cavities with high quality factors. In such an array, each unit cell consists of a resonant cavity formed by a defect and the surrounding photonic crystal lattice. The band structure of CROW structures can be readily calculated using the plane-wave expansion method [20]. Since the focus of this letter is on the operational principles of the mode-locking, we limit our optical design of the CROW to a two-dimensional structure in the transverse plane. In our design, the radius of the air-holes in the square lattice is $r_1 = 0.42a$ for a photonic lattice constant of a. A bandgap for TE modes is achieved by such a design in the frequency range of $0.276 \sim 0.306(2\pi c/a)$. The radius of the four air-holes nearest to the defect is finely tuned to $r_2 = 0.45a$ to support a single defect state (quadrapole state) lying in the middle of the band-gap per unit cell. The calculated optical field profile in a unit cell is shown in the inset of Fig. 2. In the weak-coupling regime, the dispersion relation between the supermode angular frequency ω and the Bloch wave vector K of the defect band is [6]:

$$\omega(K) = \omega_0 - \Delta\Omega - 2|\kappa| \cdot cos(KR), \tag{1}$$

where ω_0 is the optical carrier frequency, R is the length of the unit cell, i is defined as $\sqrt{-1}$, and $\Delta\Omega$ accounts for the coupling-induced frequency shift of the entire band. The coupling coefficient κ is purely imaginary, and $2|\kappa|$ determines the width of the defect band. It is straightforward to obtain the group velocity as

$$v_g(K) = \frac{d\omega}{dK} = 2|\kappa|Rsin(KR). \tag{2}$$

In our CROW design, only six lattice periods are needed in each unit cell to achieve a band width corresponding to 2meV, as shown in Fig. 2. Correspondingly, we have $R = 1.5\mu m$ for a photonic lattice constant a of $245nm$, and a maximum group velocity of $2.3 \times 10^{\,6} m/s$ at the center of the defect band.

Fig. 3 shows a schematic device configuration plot of the proposed CROW laser for mode-locking operations. The CROW has an array of resonant cavities of the total number N=50, which gives a total physical length of 75 micrometers. The corresponding supermodes intercepts the dispersion curve in Fig. 2 at N equally-spaced discrete K values. The center of the defect band has the near-zero dispersion and is used to achieve mode-locking. The frequency

#6747 - $15.00 USD Received 3 March 2005; revised 26 May 2005; accepted 31 May 2005

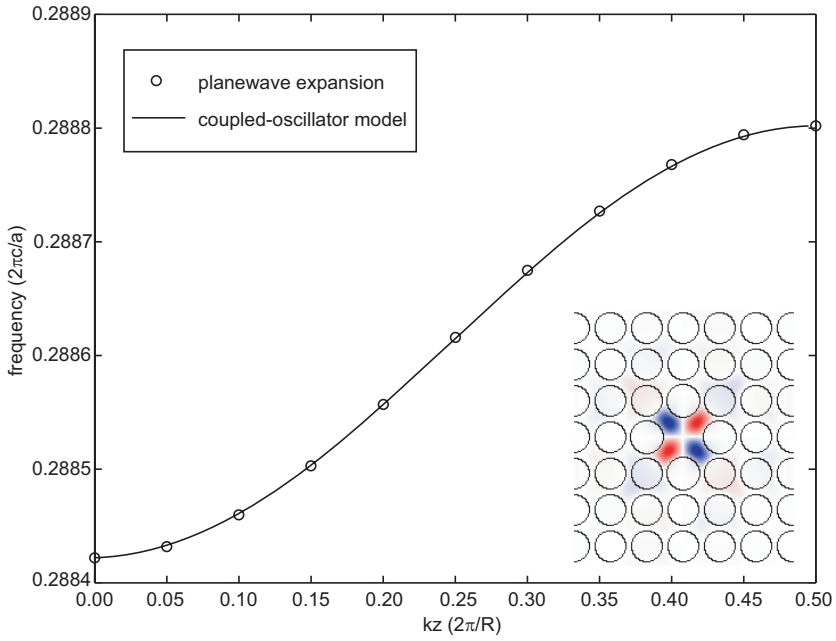

Fig. 2. Calculated defect-band dispersion relation of the proposed CROW laser diode. Calculations based on both the plane-wave expansion method [20] and the coupled-oscillator model show good agreement. The inset is the calculated field pattern of an uncoupled single resonant cavity from the plane-wave expansion method.

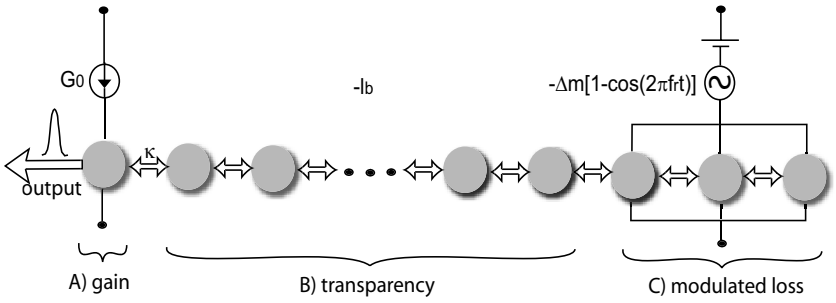

Fig. 3. Device configuration of the proposed monolithic CROW laser to achieve the mode-locking. The circles represent the resonant cavities in the CROW array as depicted in Fig. 1. The CROW array is grouped into three segments: gain, loss and modulated loss.

#6747 - $15.00 USD
Received 3 March 2005; revised 26 May 2005; accepted 31 May 2005

spacing of the two adjacent modes in this region is calculated to be 15GHz, which in turn determines the repetition frequency. As a proof of concept, we only consider active mode-locking and electrical injection schemes. Nevertheless, the CROW structure should in principle be applicable to passive mode-locking schemes using saturable absorbers or hybrid schemes and to the case of optical pumping. In our mode-locking design, the monolithic device is divided into three segments, each consisting of N_g, N_t,and N_l resonant cavities, respectively, as shown in Fig. 3. The modulated loss segment is reverse-biased by a sinusoidal radio-frequency signal at a repetition frequency $f_r = 15GHz$. It provides the necessary coupling between the adjacent supermodes, and is usually placed at one end of the device for greater modulation efficiency [4]. Furthermore, N_l should be small so that the capacitance of this segment is small enough for the radio-frequency modulation ($N_l = 4$ in this work). The gain segment is forward-biased to achieve the gain condition through electrical injection. We do not simply pump all the remaining cavities to the gain condition, because a long gain segment in the middle of the device usually leads to a preferred lasing at the band-edges, instead of stable mode-locking at the center of the band. This is found to be due to the different overlap of the standing-wave supermode profiles (Eq. (13)) with the gain/loss segments. In this work, the gain segment only consists of the first cavity. The remaining cavities can be either passive (without QWs) by design or moderately forward-biased so that the active medium reaches the transparency condition. In these cavities, photons still experience small net loss due to the intrinsic loss in the cladding layers and the scattering loss. The output coupling can be designed to occur only at the first cavity by coupling the cavity to a waveguide.

We conducted transient simulations for the mode-locked CROW lasers based on a coupled-oscillator model, which has been extensively used to study the dynamics of coupled laser arrays [16, 18, 19]. Following the approach outlined in Ref. [6], the optical field of a CROW array along the *z*-direction is expanded in the weak coupling limit as

$$\mathbf{E}(\mathbf{r},t) = e^{i\omega_0 t} \sum_{\ell=1}^{N} A_\ell(t)\mathbf{E}_\Omega(\mathbf{r} - \ell R\mathbf{e}_z), \tag{3}$$

where the expansion basis fields, $\mathbf{E}_\Omega(\mathbf{r} - \ell R\mathbf{e}_z)$ for $\ell = 1, 2, \cdots, N$, are the individual cavity modes. $\mathbf{E}(\mathbf{r},t)$ satisfies

$$\nabla \times (\nabla \times \mathbf{E}(\mathbf{r},t)) = -\frac{1}{c^2}\varepsilon(\mathbf{r},t)\frac{\partial^2}{\partial t^2}\mathbf{E}(\mathbf{r},t), \tag{4}$$

where $\varepsilon(\mathbf{r},t)$ is the permittivity of the CROW system including the gain/loss. We have adopted the adiabatic approximation that the gain/loss changes slowly compared to the optical frequency ω_0. For $\mathbf{E}_\Omega(\mathbf{r})$ we have

$$\nabla \times (\nabla \times \mathbf{E}_\Omega) = \varepsilon_0(\mathbf{r})\frac{\omega_0^2}{c^2}\mathbf{E}_\Omega, \tag{5}$$

where $\varepsilon_0(\mathbf{r})$ is the unperturbed permittivity of the single cavity resonator. By doing so, we have assumed that the individual cavity modes form a complete basis set in the tight-binding approach, which is also an underlying assumption in the work of [6, 12, 19]. This assumption is valid for the weakly coupled CROW lasers studied here because the entire defect band is deep within the photonic band gap; the perturbation due to the continuum states can therefore be neglected as discussed in [23]. In the case that the resonators are strongly coupled, the continuum states need to be considered [21, 22]. We also note that $\mathbf{E}_\Omega$'s do not form an orthogonal set, which has been fully accounted for in our following derivations. The permittivity of the coupled system in Eq. (4) can be expressed as

$$\varepsilon(\mathbf{r},t) = \bar{\varepsilon}(\mathbf{r}) + \Delta\varepsilon(\mathbf{r},t) = \bar{\varepsilon}(\mathbf{r}) + \sum_{\ell=1}^{N} \Delta\varepsilon_\ell(\mathbf{r},t) \tag{6}$$

#6747 - $15.00 USD Received 3 March 2005; revised 26 May 2005; accepted 31 May 2005

where the perturbation $\Delta\varepsilon_\ell(\mathbf{r},t)$ accounts for the gain/loss in the ℓ-th cavity. In Eq. (3), $\mathbf{E}_\Omega(\mathbf{r})$ is normalized ($\int d^3\mathbf{r}\varepsilon_0(\mathbf{r})\mathbf{E}_\Omega\cdot\mathbf{E}_\Omega = 1$), so that $N_{ph,\ell}(t) = |A_\ell(t)|^2$ is the photon number in that cavity at time t, which is also a slowly-varying quantity compared to ω_0. After substituting Eq. (3) into Eq. (4) and using Eq. (5), one can obtain

$$\begin{aligned}\frac{2i}{\omega_0}\sum_{\ell=1}^{N}\big[\bar{\varepsilon}(\mathbf{r})+\Delta\varepsilon(\mathbf{r},t)\big]\mathbf{E}_\Omega(\mathbf{r}-\ell R\mathbf{e}_z)\frac{dA_\ell}{dt} &= \sum_{\ell=1}^{N}\big[\bar{\varepsilon}(\mathbf{r})-\varepsilon_0(\mathbf{r}-\ell R\mathbf{e}_z)\big]\mathbf{E}_\Omega(\mathbf{r}-\ell R\mathbf{e}_z)A_\ell \\ &\quad+\sum_{\ell=1}^{N}\Delta\varepsilon(\mathbf{r},t)\mathbf{E}_\Omega(\mathbf{r}-\ell R\mathbf{e}_z)A_\ell\end{aligned} \tag{7}$$

Multiplying Eq. (7) by $\mathbf{E}_\Omega(\mathbf{r}-mR\mathbf{e}_z)$ and spatially integrating, a set of equations can be obtained in the matrix form as

$$\big(\tilde{\tilde{\mathbf{a}}}+\tilde{\tilde{\mathbf{d}}}\big)\frac{\partial\tilde{\mathbf{A}}}{\partial t} = \frac{\omega_0}{2i}\big(\tilde{\tilde{\mathbf{c}}}+\tilde{\tilde{\mathbf{d}}}\big)\tilde{\mathbf{A}}, \tag{8}$$

where $\tilde{\mathbf{A}} = [A_1, A_2, \cdots, A_N]^t$ is a column vector, and $\tilde{\tilde{\mathbf{a}}}, \tilde{\tilde{\mathbf{c}}}, \tilde{\tilde{\mathbf{d}}}$ are $N\times N$ matrices with their elements given by

$$\begin{aligned} a_{\ell,m} &= \int d^3\mathbf{r}\bar{\varepsilon}(\mathbf{r})\mathbf{E}_\Omega(\mathbf{r}-\ell R\mathbf{e}_z)\cdot\mathbf{E}_\Omega(\mathbf{r}-mR\mathbf{e}_z) \\ c_{\ell,m} &= \int d^3\mathbf{r}\big[\bar{\varepsilon}(\mathbf{r})-\varepsilon_0(\mathbf{r}-\ell R\mathbf{e}_z)\big]\mathbf{E}_\Omega(\mathbf{r}-\ell R\mathbf{e}_z)\cdot\mathbf{E}_\Omega(\mathbf{r}-mR\mathbf{e}_z) \\ d_{\ell,m} &= \int d^3\mathbf{r}\Delta\varepsilon(\mathbf{r},t)\mathbf{E}_\Omega(\mathbf{r}-\ell R\mathbf{e}_z)\cdot\mathbf{E}_\Omega(\mathbf{r}-mR\mathbf{e}_z). \end{aligned} \tag{9}$$

In the weak-coupling regime, $\tilde{\tilde{\mathbf{a}}}$ is diagonal dominant and can be expressed as $\tilde{\tilde{\mathbf{a}}} = \tilde{\tilde{\mathbf{I}}} + \tilde{\tilde{\mathbf{a}}}'$, where $\tilde{\tilde{\mathbf{I}}}$ is an $N\times N$ identity matrix. The three matrices, $\tilde{\tilde{\mathbf{a}}}', \tilde{\tilde{\mathbf{c}}}$, and $\tilde{\tilde{\mathbf{d}}}$, are small perturbations. Therefore, Eq. (8) can be rewritten to the first order accuracy as

$$\frac{\partial\tilde{\mathbf{A}}}{\partial t} = \frac{\omega_0}{2i}\big(\tilde{\tilde{\mathbf{I}}}+\tilde{\tilde{\mathbf{a}}}'+\tilde{\tilde{\mathbf{d}}}\big)^{-1}\big(\tilde{\tilde{\mathbf{c}}}+\tilde{\tilde{\mathbf{d}}}\big)\tilde{\mathbf{A}} \approx \frac{\omega_0}{2i}\big(\tilde{\tilde{\mathbf{I}}}-\tilde{\tilde{\mathbf{a}}}'-\tilde{\tilde{\mathbf{d}}}\big)\big(\tilde{\tilde{\mathbf{c}}}+\tilde{\tilde{\mathbf{d}}}\big)\tilde{\mathbf{A}} \approx \frac{\omega_0}{2i}\big(\tilde{\tilde{\mathbf{c}}}+\tilde{\tilde{\mathbf{d}}}\big)\tilde{\mathbf{A}} \tag{10}$$

Considering only the nearest-neighbor coupling and to the first order accuracy, the only non-trivial matrix elements in the final expression of Eq. (10) are

$$\begin{aligned} -i\Delta\Omega \equiv \frac{\omega_0}{2i}c_{\ell,\ell} &= \frac{\omega_0}{2i}\int d^3\mathbf{r}\big[\bar{\varepsilon}(\mathbf{r})-\varepsilon_0(\mathbf{r})\big]\mathbf{E}_\Omega(\mathbf{r})\cdot\mathbf{E}_\Omega(\mathbf{r}) \\ \kappa \equiv \frac{\omega_0}{2i}c_{\ell,\ell\pm1} &= \frac{\omega_0}{2i}\int d^3\mathbf{r}\big[\bar{\varepsilon}(\mathbf{r})-\varepsilon_0(\mathbf{r})\big]\mathbf{E}_\Omega(\mathbf{r})\cdot\mathbf{E}_\Omega(\mathbf{r}-R\mathbf{e}_z) \\ \frac{\omega_0}{2i}d_{\ell,\ell} &= \frac{\omega_0}{2i}\int d^3\mathbf{r}\Delta\varepsilon_\ell(\mathbf{r},t)\mathbf{E}_\Omega(\mathbf{r}-\ell R\mathbf{e}_z)\cdot\mathbf{E}_\Omega(\mathbf{r}-\ell R\mathbf{e}_z), \end{aligned} \tag{11}$$

for $\ell = 1, 2, \cdots, N$. The real and imaginary parts of $(\omega_0/2i)d_{\ell,\ell}$ correspond to the net gain and the gain induced frequency shift, respectively. Considering the configurations of the mode-locked CROW lasers, the following set of rate equations are therefore obtained:

$$\frac{dA_\ell(t)}{dt} = \kappa[A_{\ell-1}(t)+A_{\ell+1}(t)] + i(\Delta\omega_\ell-\Delta\Omega)A_\ell + \big[\frac{G_\ell(t)}{2}-\delta_{\ell,1}\gamma\big](1-i\alpha)A_\ell(t)+S_\ell(t), \tag{12}$$

for $\ell = 1, 2, \cdots, N$. The net gain $G_\ell(t)$ and the spontaneous emission source $S_\ell(t)$ are both dependent on time and cavity index. γ is the output coupling loss applied to the first cavity. The

#6747 - $15.00 USD Received 3 March 2005; revised 26 May 2005; accepted 31 May 2005

amplitude phase coupling effect associated with cavity gain/loss is described by the linewidth enhancement factor [24], $\alpha \equiv -(\partial\varepsilon'/\partial n_c)/(\partial\varepsilon''/\partial n_c)$, where ε' and ε'' are the real and imaginary part of the complex permittivity and n_c is the carrier density in the active region. $\Delta\omega_\ell$ is the detuning of the ℓ-th cavity in the CROW design, which is assumed to be zero unless otherwise noted. For passive CROWs with boundary conditions $A_0(t) = A_{N+1}(t) = 0$, the supermodes are obtained by diagonalizing the coupling matrix as

$$\mathbf{E}_K(\mathbf{r}) = \sum_{\ell=1}^{N} sin(\ell RK)\mathbf{E}_\Omega(\mathbf{r} - \ell R\mathbf{e}_z). \tag{13}$$

The discrete wavevectors are $K = m\pi/(N+1)R$ for $m = 1, 2, \cdots, N$ and the dispersion relation is again obtained as $\omega_K = \omega_0 - \Delta\Omega - 2i\kappa \cdot cos(KR)$. As shown in Fig. 2, the dispersion relation obtained from the coupled-oscillator model matches with that from exact numerical calculations, which strongly indicates the validity of our analytical approach.

In treating the mode-locking process, the net gain is accounted for according to the device configuration as shown in Fig. 3, following the approach outlined in [25]:

$$G_\ell(t) = \begin{cases} G(t), & \text{gain segment} \\ -l_b, & \text{transparency segment} \\ -\Delta m[1 - cos(2\pi f_r t)], & \text{modulated loss segment,} \end{cases} \tag{14}$$

for $\ell = 1, 2, \cdots, N$. For the gain segment that only consists the first cavity, we assume the gain is frequency independent instead of using a parabolic gain dispersion model as in [25]. This is valid since the total bandwidth of the defect band is $2meV$, far smaller than the material gain bandwidth that is at the order of the thermal energy ($25meV$ at room temperature). The gain dynamics is accounted for based on the carrier continuity equation [26]:

$$\frac{dN_c(t)}{dt} = \frac{I_0}{q} - \frac{N_c(t)}{\tau_c} - G(t) \cdot N_{ph}(t), \tag{15}$$

where $N_c(t)$ and $N_{ph}(t)$ are the carrier and photon numbers in the cavity, respectively, I_0 is the drive current, q is the elementary charge, and τ_c is the carrier lifetime due to both radiative (spontaneous) and non-radiative recombination processes. We have $1/\tau_c = 1/\tau_r + 1/\tau_{nr}$, where τ_r and τ_{nr} are radiative and non-radiative carrier lifetimes, respectively. The contribution from stimulated recombinations is included in the term $G(t) \cdot N_{ph}(t)$. The modal gain, $G(t)$, is related to the material gain, $g(t)$, as $G(t) = (c/n_r) \cdot \Gamma \cdot g(t)$, where Γ is the optical confinement factor. In relating $g(t)$ to the carrier density $n(t)$, we adopt a linear expression to approximate the realistic material gain of $GaAs/AlGaAs$ QWs as follows [26]

$$g(t) = g' \cdot (n(t) - n_{tr}), \tag{16}$$

where n_{tr} is the transparency carrier density and g' is the differential material gain. The relation between the carrier number, $N_c(t)$, and the carrier density, $n(t)$ is given by $N_c(t) = n(t) \cdot d \cdot s$, where d is the thickness of the QWs and s is the area of the active region. By using these relations, we can therefore re-write Eq. (15) and obtain a rate equation for $G(t)$ as:

$$\frac{dG(t)}{dt} = \frac{1}{\tau_c}\left[G_0 - G(t) - \Theta \cdot |A(t)|^2 \cdot G(t)\right], \tag{17}$$

where the pumping rate G_0 is expressed as

$$G_0 = \Gamma \cdot (c/n_r) \cdot g' \cdot \left(\frac{\tau_c \cdot I_0}{q \cdot d \cdot s} - n_{tr}\right), \tag{18}$$

#6747 - $15.00 USD Received 3 March 2005; revised 26 May 2005; accepted 31 May 2005

and the photon gain coupling coefficient Θ is given by

$$\Theta = \frac{\tau_c \cdot \Gamma \cdot (c/n_r) \cdot g'}{d \cdot s}. \tag{19}$$

The transparency segment is associated with a small amount of the background loss l_b. For the modulated loss segment, Δm is the modulation depth, and f_r is the modulation frequency. The modulation frequency is set equal to the beat frequency of the supermodes at the center of the defect band to enable their coherent beating. We only consider the spontaneous emission contribution in the gain segment, which is treated as a Langevin force $S_\ell(t)$ taken as white Gaussian noise that obeys $< S_\ell(t) >= 0$ and $< S_\ell(t) S_\ell^*(t-\tau) >= (R_{sp}/2)\delta(\tau)$, where $<>$ is for the ensemble average and $\delta(t)$ is the Dirac function [24]. In this expression, the spontaneous emission rate at the lasing frequency, R_{sp}, is approximated by $R_{sp} \approx \beta \cdot n_0 \cdot d \cdot s/\tau_r$, where β is the fraction of the spontaneous emission coupled into the cavity mode, and $n_0 = \tau_c \cdot I_0/(q \cdot d \cdot s)$ is the threshold carrier density.

3. Numerical results and discussions

The numerical simulation of Eq. (12) and Eq. (17) is carried out by a time-marching method with a time interval $\Delta t = 2.6 \times 10^{-14} s$. In particular, the Langevin force term for the first cavity is treated as $S_1(t) = \chi_e \sqrt{R_{sp}/(2\Delta t)}$ in each time interval of the simulation, where χ_e is a complex Gaussian random variable with zero mean and unit variance [27]. The initial condition of the simulation is $G(t=0) = 0$ for the first cavity and $A_\ell(t=0) = 0$ for $\ell = 1, 2, \cdots, N$. The values of the simulation parameters are listed in Table 1. The modal values of the loss parameters are used in the simulation. We also list their corresponding material values in the table, which are obtained by dividing the modal values by $\Gamma c/n_r$. All the material parameters are typical for unstrained $GaAs/Al_{0.2}Ga_{0.8}As$ 80Å QWs [26]. The QW's non-radiative recombination lifetime τ_{nr} results from Shockley-Read-Hall and Auger recombination processes and is about $10^{-7} - 10^{-6} s$ for good quality QWs under moderate injection levels [28]. We use a short τ_{nr} of $1ns$ in the simulation to account for strong surface recombination induced by the photonic lattice hole-etching process. The spontaneous emission coupling coefficient, β, can be significantly enhanced for defect states within a photonic bandgap from its conventional value of 10^{-4} to as large as 0.4 [29]; we use a β value of 0.01 in the simulation. The linewidth enhancement factor α is important for stable mode-locked operations and the range of its typical values is $2 \sim 5$ for QW laser diodes [30], depending on lasing wavelength, QW and barrier material compositions and strains. In this work, simulation results are presented for both $\alpha = 2$ and $\alpha = 5$.

Time-dependent optical intensity distributions from numerical simulations for $\alpha = 2$ are shown in Fig. 4. The sub-figures plot the photon number inside the individual cavities of the CROW at different time instances. The photon number distribution has the form of a random noise at the initial stage (Fig. 4(a)). It evolves under the combined effects of gain, background and modulated losses, spontaneous emission and nearest neighbor couplings. An optical pulse is shown to emerge from the random noise background at $2.763ns$ in Fig. 4(b), indicating the effect of active mode-locking. As can be seen from the photon number distribution at three different time instances around $15.8ns$ in Fig. 4(c), an optical pulse is observed to propagate along the CROW array. This gives clear evidence of mode-locking, i.e. the coherent beating of several supermodes at a beat frequency f_r. The peak intensity of the pulse is decreasing as the pulse propagates away from the gain segment (the left end), due to the background and modulated losses. This pulse bounces back as it hits the ends of the device, travels back to the gain segment, and gets re-amplified, so that the cw operation is maintained.

In Fig. 5(a), the simulated temporal optical output power from the output coupling of the first cavity is shown. The optical output power is obtained by $P_{out}(t) = 2\gamma |A_1(t)|^2 hc/\lambda_0$, where h is

#6747 - $15.00 USD Received 3 March 2005; revised 26 May 2005; accepted 31 May 2005

Table 1. Parameter values used in the numerical simulations. For the loss parameters, both their modal and material values are listed.

Parameter	Symbol	Value
photonic lattice constant	a	$245nm$
air-hole radius	r_1	$0.42a$
air-hole radius near defect	r_2	$0.45a$
inter-cavity distance	R	$1.5\mu m$
nominal lasing wavelength	λ_0	$850nm$
QW thickness	d	$80Å$
active region area	s	$(2a)^2$
total cavity number	N	50
total device length	L	$75\mu m$
repetition frequency	f_r	$15GHz$
optical confinement factor	Γ	0.03
vacuum light speed	c	$3\times10^8 m/s$
effective refractive index	n_r	3.5
background loss	l_b	$7.5\times10^9/s(30/cm)$
modulation depth	Δm	$3.8\times10^{11}/s(1465/cm)$
cavity coupling coeff.	$i\kappa$	$7.6\times10^{11}/s$
linewidth enhancement factor	α	2 or 5
differential material gain	g'	$0.8\times10^{-19}m^2$
transparency carrier density	n_{tr}	$2.6\times10^{18}cm^{-3}$
drive current (1st cav.)	I_0	$3.6\mu A$
elementary charge	q	$1.6\times10^{-19}C$
carrier lifetime	τ_c	$0.5ns$
radiative carrier lifetime	τ_r	$1ns$
non-rad. carrier lifetime	τ_{nr}	$1ns$
spon. emission coupling coeff.	β	0.01
output coupling loss (1st cav.)	γ	$3.8\times10^{11}/s$

the Planck constant. A turn-on delay is evident in the figure, which is due to the finite gain build-up time. After the gain builds up, the output power initially exhibits irregular pulsations. The mode-locking mechanism purifies the pulses and a train of clean output pulses is achieved after $\sim 4ns$. An oscillation behavior is also observed in the amplitude envelope of the pulse train, which is due to the relaxation oscillation commonly observed in laser transients. A close-up view of the output pulse train at the CW condition is given in Fig. 5(b). The output pulses exhibit a period equal to the inverse of f_r. Figure 6 shows a curve fit to one of the pulses with a temporal Gaussian profile $P_{out}(t) = exp(-2t^2/\sigma^2)$ [4]. The fitting gives a σ value of $5.2ps$, and a full-width half-maximum of $\sqrt{2ln2}\sigma = 6.2ps$ is thus obtained. The simulated dynamics of the modal gain in the first cavity is plotted in Fig. 7. The turn-on delay and relaxation oscillations are also evident in the envelope of the gain amplitudes. In a close-up view shown in the inset of the figure, one can see a rapid oscillation of the modal gain at a rate equal to the repetition frequency f_r. This is explained by the gain depletion due to optical pulses and the finite gain recovery time.

Simulations are also carried out for the proposed CROW device with the same numerical parameters, except for a large linewidth enhancement factor, $\alpha = 5$. The simulated time-dependent

#6747 - $15.00 USD Received 3 March 2005; revised 26 May 2005; accepted 31 May 2005

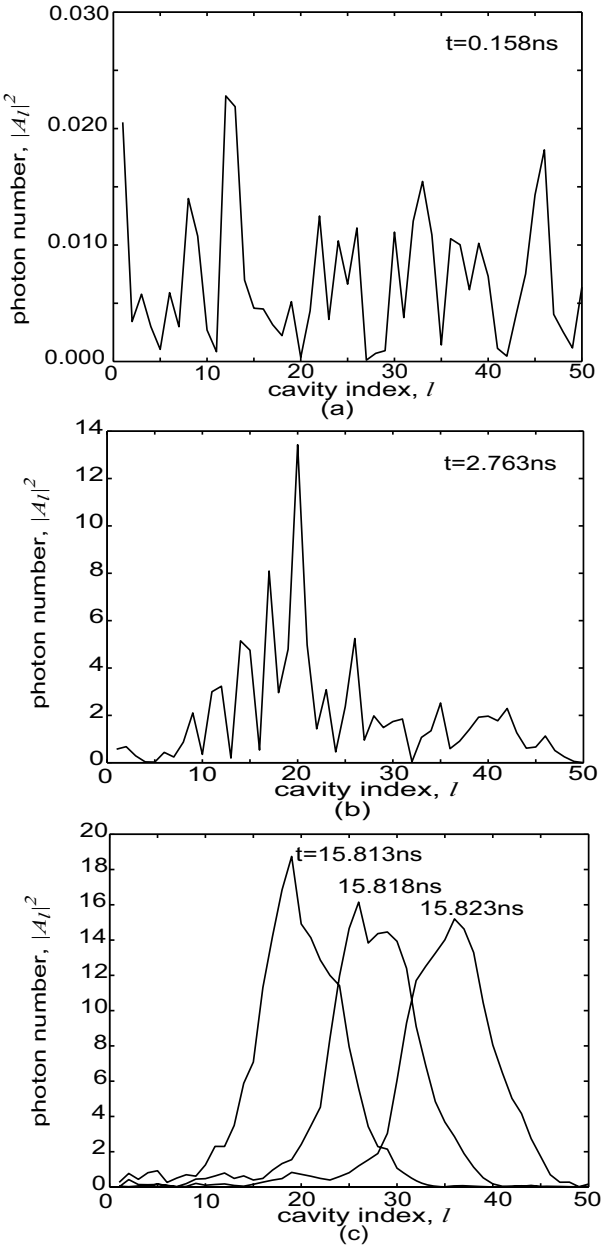

Fig. 4. Simulated transient behavior of the photon number distribution in the resonant cavities of the CROW array at three stages: (a) initial stage; (b) intermediate stage; (c) cw mode-locking. The propagation of an optical pulse is evident in (c), indicating the action of mode locking. The inter-cavity distance is $R = 1.5\mu m$. The linewidth enhancement factor $\alpha = 2$.

#6747 - $15.00 USD Received 3 March 2005; revised 26 May 2005; accepted 31 May 2005

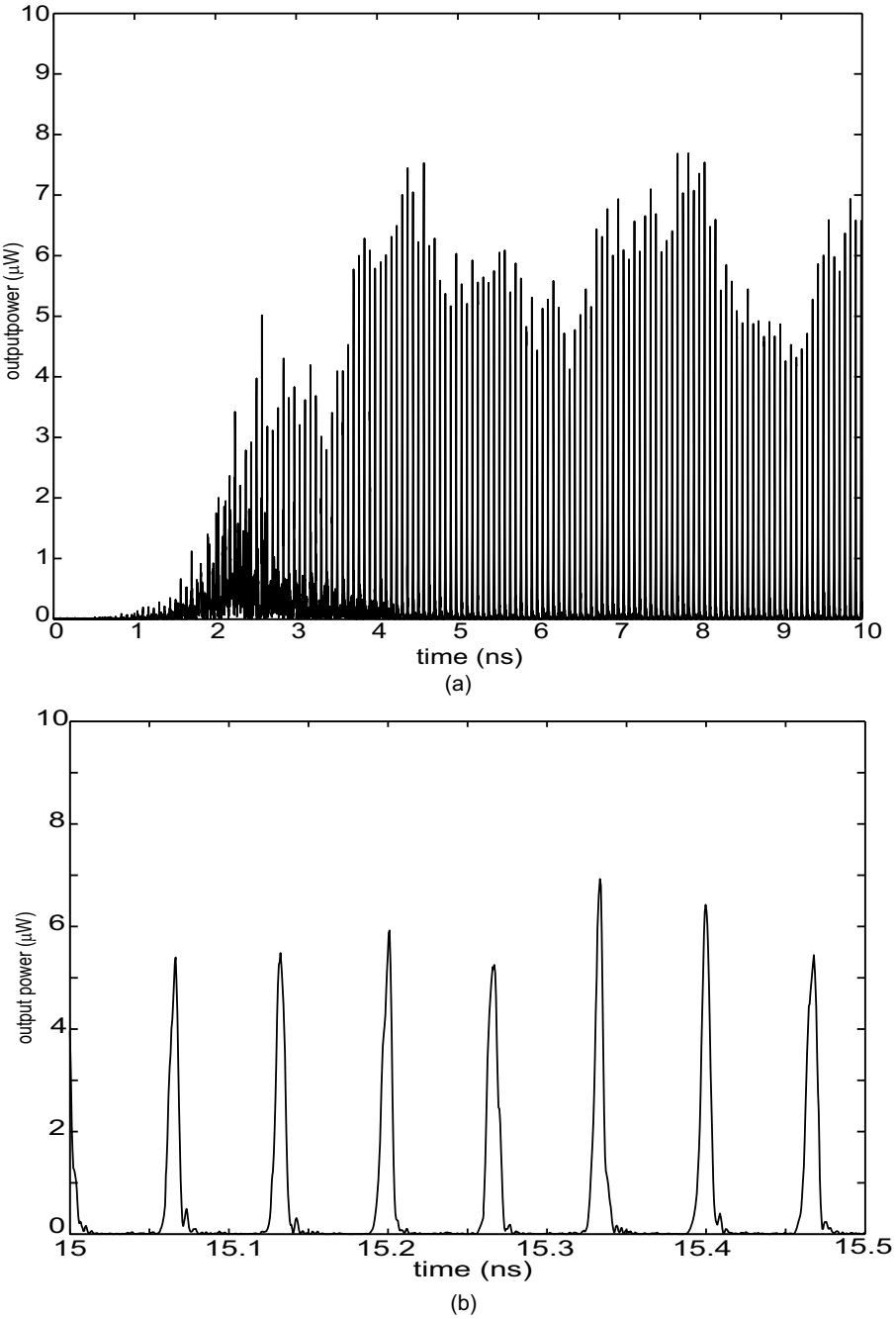

Fig. 5. (a) Simulated time-dependent optical output power from the output coupling of the first cavity; (b) a close-up view. The linewidth enhancement factor is $\alpha = 2$.

#6747 - $15.00 USD Received 3 March 2005; revised 26 May 2005; accepted 31 May 2005

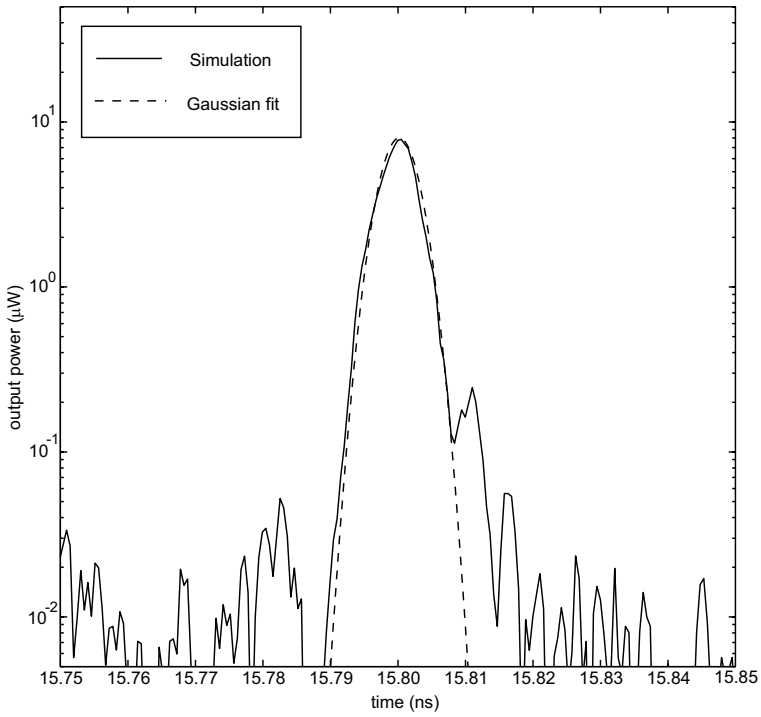

Fig. 6. A Gaussian fit of a simulated optical pulse at the cw condition in Fig. 5 (note the log scale in the output power). The FWHM of the pulse is found to be 6.2 ps.

output optical power from the output coupling of the first cavity is given in Fig. 8(a). Figure 8(b) provides a close-up view of it in a short time window. It is evident that severe instabilities are introduced due to the large α parameter. The periodic mode-locked optical pulses are distorted by irregular pulsations. Such behavior is very similar to that revealed in early works regarding the instability of phase-locked laser arrays [14, 16]. The underlying cause is a strong amplitude phase coupling as characterized by the large α parameter. In a coupled-oscillator picture as described by Eq (12), a frequency pulling effect occurs in those cavities with net gain or loss; its amount is determined by the product of α and the net modal gain or loss. A large α parameter may significantly shift the resonant frequencies of the cavities in the gain and modulated loss segments, which reduces their coupling with those in the transparency region and hence degrades the mode-locking operation. Nevertheless, such instabilities can be effectively suppressed by introducing small resonant frequency detunings for individual cavities in CROW designs. For the first cavity that supplies the net gain, a frequency detuning is needed to offset the difference between the gain level at the cw condition and γ, with the multiplication by the α parameter taken into account. For those cavities in the modulated loss segment, a frequency detuning that is equal to $\Delta m \cdot \alpha$ is desired. By doing so, the cavities in that segment are in resonant with those in the transparency segment when the modulated loss is at its peak value, so that its shaping of optical pulses can be effective. Based on these considerations, we performed simulations for $\alpha = 5$ with frequency detunings $\Delta\omega_1 = 0.7 \times 10^{12}\ Rad/s$ applied to the first cavity and $\Delta\omega_N = 1.9 \times 10^{12}\ Rad/s$ to the last four cavities. The simulated temporal output power from the first cavity is again plotted in Fig. 9(a). A close-up view of it is also given in Fig. 9(b). It is evident that after incorporating these small frequency detunings in the CROW design, a clean, periodic optical pulse train is obtained and the mode-locking behavior is fully

#6747 - $15.00 USD Received 3 March 2005; revised 26 May 2005; accepted 31 May 2005

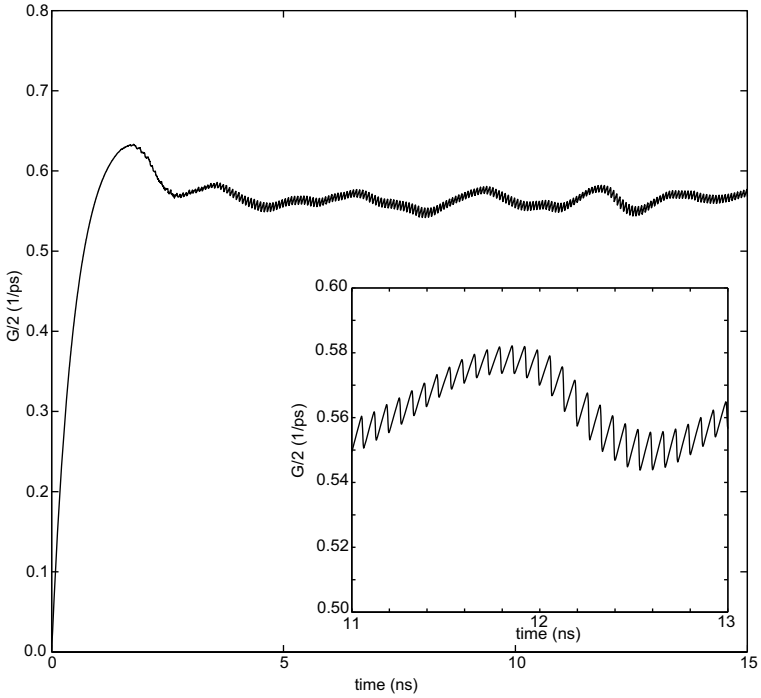

Fig. 7. Simulated time-dependent optical amplitude gain in the first cavity. The inset is a close-up view. The linewidth enhancement factor $\alpha = 2$.

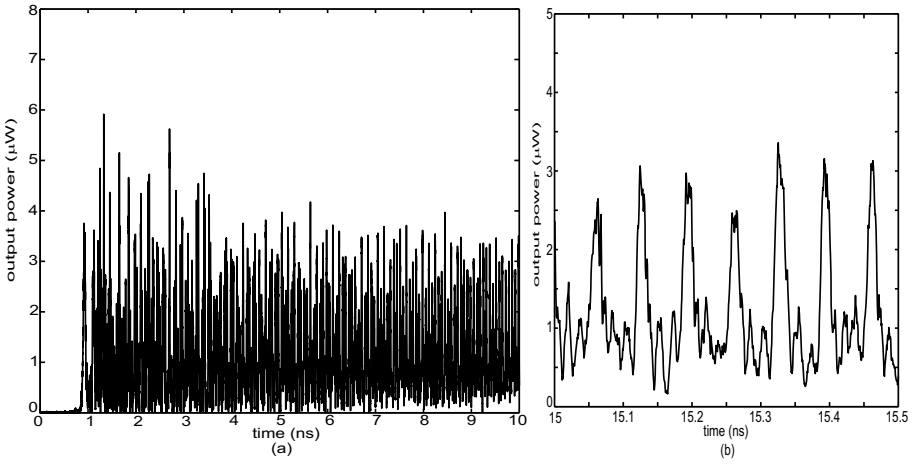

Fig. 8. (a) Simulated time-dependent optical output power from the output coupling of the first cavity; (b) a close-up view. The linewidth enhancement factor is $\alpha = 5$.

#6747 - $15.00 USD Received 3 March 2005; revised 26 May 2005; accepted 31 May 2005

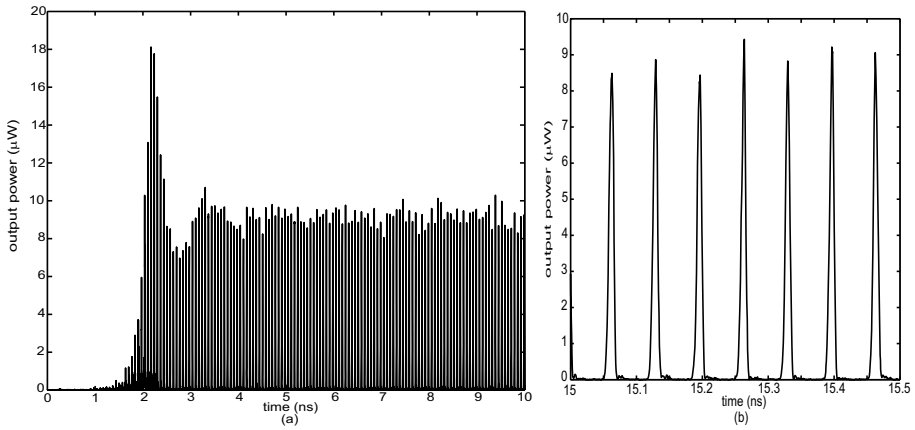

Fig. 9. (a) Simulated time-dependent optical output power from the output coupling of the first cavity; (b) a close-up view. The linewidth enhancement factor is $\alpha = 5$. Frequency detunings in the first and the last four cavities are incorporated.

recovered even for the large α parameter. In practice, a proper amount of frequency detuning should be incorporated at the stage of the actual CROW design; the injection current and the modulation depth can be two adjustable parameters to ensure stable operation. We further note that thermal effects should also be carefully considered in device design. Non-negligible cavity frequency shift may be induced in the active cavities due to elevated lattice temperature at high injection levels. We expect the self-heating effect combined with the fact that the active area is small in such devices will limit their maximum power, as is the case in most micro-cavity lasers. Good thermal management can be a key factor to achieve relatively high power in such devices.

4. Conclusions

We have numerically investigated the operational principles of mode-locking in monolithic laser diodes incorporating CROW structures. We base our transient simulations on a coupled-oscillator model to describe the photon dynamics and an additional rate equation to account for the gain dynamics. The numerical simulations have clearly demonstrated the action of mode-locking in the proposed structures. The proposed device length is only $75\mu m$ at a repetition rate of $15GHz$, which is a drastic reduction from the several millimeters in conventional mode-locked lasers at the same repetition rate. The impact of amplitude phase coupling on the stability of mode-locking has also been investigated. It is found that the mode-locking behavior is stable for moderate values of the linewidth enhancement factor. Instabilities are associated with large values of the linewidth enhancement factor, which may severely degrade the mode-locking behavior and result in irregular pulsations. Nevertheless, it has been demonstrated that such instabilities can be effectively suppressed by proper design of cavity frequency detuning.

Acknowledgments

We thank Prof. J. Harris, R. Aldaz, M. Wiemer at Stanford for stimulating discussions on mode-locked lasers. This work was supported under the MARCO Interconnect Focus Center project.

#6747 - $15.00 USD Received 3 March 2005; revised 26 May 2005; accepted 31 May 2005